Applied Surface Science 480 (2019) 998–1007

Contents lists available at ScienceDirect

Applied Surface Science

journal homepage: www.elsevier.com/locate/apsusc

Full length article

The influence of surface pre-twinning on the friction and wear performance of an AZ31B Mg alloy

Bo Mao[a], Arpith Siddaiah[a], Xing Zhang[a], Bin Li[b], Pradeep L. Menezes[a,*], Yiliang Liao[a,*]

[a] Department of Mechanical Engineering, University of Nevada, Reno, Reno, NV 89557, USA
[b] Department of Chemical and Materials Engineering, University of Nevada, Reno, Reno, NV 89557, USA

ARTICLE INFO

Keywords:
Friction
Wear
Magnesium alloys
Deformation twins

ABSTRACT

Twinning is an important mode in plastic deformation of hexagonal close-packed magnesium (Mg) alloys that are promising lightweight structural metals. Recent studies show that the hardness, strength, and stretch formability of Mg alloys can be improved by pre-twinning. However, how twinning and associated microstructure influence the tribological properties of Mg alloys have not been studied systematically. In this work, a gradient twin microstructure in which the density of twins decreases with depth was introduced to an AZ31B Mg alloy plate by laser shock peening. Then sliding tests were performed on surfaces with varying twin volume fraction (TVF) under dry condition. The results shown that both the coefficient of friction (COF) and wear rate decrease with the increase of TVF. A possible mechanism responsible for the effect of surface pre-twinning on the tribo-performance of Mg alloys is proposed. In specific, it is discussed that the improved tribo-performance of Mg alloys by pre-twinning are attributed to the twinning-induced hardening effect, twin growth and saturation phenomenon, and twinning-induced surface crystallographic texture change during sliding. We envision the results in the present study can offer new insights on the designing and developing Mg alloys towards enhanced tribological performance.

1. Introduction

Magnesium (Mg) and its alloys offer lightweight alternatives to conventional metallic materials due to their good strength-to-weight ratio, machinability and recyclability [1,2]. However, their potential applications are currently restricted due to their poor formability, limited ductility and low wear resistance at room temperature [3–5]. New alloy design and processing strategies have been developed in recent years in order to overcome these barriers [6–8], while most of them aim to improve the ductility and/or strength of Mg alloys. In some applications, such as pistons, valves, bearing, sliding seals and gears, Mg alloys are subjected to sliding motion where friction and wear performance is of specific importance [9]. Moreover, sliding wear is an important consideration in the forming process of Mg alloys, such as drawing, extrusion and forging [10]. Therefore, improving the tribological properties of Mg alloys is of critical importance for expanding their engineering applications.

Several studies have been conducted to investigate the tribological properties of Mg alloys as affected by various tribological conditions including applied load, sliding speed, temperature and lubricated conditions [10–17]. For instance, Anbu et al. [12] studied the wear mechanism of a casted ZE41A Mg alloy. Five wear mechanisms were proposed including abrasion, oxidation, delamination, plastic deformation, and melting. Taltavull et al. [13] investigated the effects of applied load and sliding speed on the wear behavior of an AM50 Mg alloy. It was found that the wear behavior transitioned from abrasion and adhesion to severe plastic deformation with increasing applied load and sliding velocity. Liang et al. [18] explored the correlation between friction-induced microstructural evolution and tribological properties of AZ31 Mg alloys. It was found that a solidified layer formed beneath the worn surface followed by a dynamic recrystallization zone and a deformed zone.

Besides these scientific studies, several strategies have been developed to improve the tribological performance of Mg alloys, either by fabricating a hard surface coating or introducing a nano-crystallization surface layer. For instance, Yu et al. [19] utilized a plasma electrolytic oxidation method to fabricate SiC based coatings on the surface of an AZ31 Mg alloy. The wear rates of the coated Mg alloy samples were reduced by 75% as compared with the untreated ones. Wang et al. [20] developed a laser cladding approach to fabricate Al—Si coatings on the surface of an AZ91 Mg alloy. The results showed that the wear rate can be significantly decreased by laser cladding. Sun et al. [15] carried out

* Corresponding authors.
E-mail addresses: pmenezes@unr.edu (P.L. Menezes), yliao@unr.edu (Y. Liao).

https://doi.org/10.1016/j.apsusc.2019.03.070
Received 3 October 2018; Received in revised form 29 December 2018; Accepted 7 March 2019
Available online 08 March 2019
0169-4332/

a surface mechanical attrition treatment on an AZ91D Mg alloy and found that the coefficient of friction (COF) of the processed samples can be reduced by 15% with the presence of nano-grains.

Despite the aforementioned studies, little attention has been placed on investigating how the tribo-performance of Mg alloys is affected by deformation twinning, which is the prevalent plastic deformation mechanism in Mg alloys due to their limited slip systems at ambient temperature [21]. Twins are lenticular grains with a different but well-defined crystallographic orientation from the parent grain activated typically by a homogeneous simple shear [22]. Among the multiple modes, $\{10\bar{1}2\}\langle 10\bar{1}\bar{1}\rangle$ extension twinning is the most commonly observed twinning mode in Mg alloys. Recent studies show that the pre-existing $\{10\bar{1}2\}\langle 10\bar{1}\bar{1}\rangle$ twins can effectively improve the surface hardness [23], tensile strength [24], and stretch formability [25] of Mg alloys. It is of specific scientific and technical importance to investigate the effect of surface pre-twinning on the friction and wear performance of Mg alloys.

This research aims to understand the friction and wear properties of Mg alloys as affect by deformation twinning. AZ31B Mg alloy samples with various twin volume fraction (TVF) are prepared by laser shock processing. Sliding tests under dry condition are conducted for friction and wear testing. The COF values and wear tracks are measured and analyzed. The relationship among the TVF, COF, and wear resistance are discussed. A possible mechanism responsible for the effect of TVF on the tribo-performance of Mg alloys is proposed. We envision the results in the present study can offer new insights on designing and developing Mg alloys towards enhanced tribological performance.

2. Experimental details

2.1. Laser shock peening

Laser shock peening (LSP) is a laser-based surface processing technique which utilizes high energy laser pulses to introduce compressive residual stresses and surface work-hardened layer to improve the durability of metallic materials [26,27]. In the LSP process, the target is typically covered by an ablative coating and a transparent confinement layer. Due to the laser-matter interaction, the ablative coating layer is evaporated and ionized, leading to the formation of laser-induced plasma [28]. The hydrodynamic expansion of plasma is restricted by the transparent confinement, resulting in a shockwave with a high peak pressure (on the order of GPa) propagating into the target material. When the pressure of the shockwave exceeds the dynamic yield strength of the target material, plastic deformation with an ultra-high strain rate (10^5–10^6/s) is induced on the surface [29,30], leading to the generation of compressive residual stresses and work-hardened layer. LSP has been widely used to enhance the engineering performance of metallic materials by increasing their surface strength, fatigue endurance, wear resistance, and stress corrosion resistance [31–33].

2.2. Preparation of Mg alloy samples with various TVFs by LSP

Rolled AZ31B Mg alloy plate purchased from Metalmart International Inc. was used for our experiments. Square plate samples with a width of 25 mm and a thickness of 10 mm were cut and then processed by laser shock peening (LSP) to prepare samples with various TVFs. Prior to LSP, sample surfaces were grinded using SiC sandpapers with different grit numbers (from 320 to 1200), followed by fine polishing using 3 μm diamond suspension. LSP experiments were conducted with a laser intensity of 1.5 GW/cm^2 along the rolled direction (RD) of the sample. The schematic view of LSP configuration is shown in Fig. 1a. In this study, a Q-switched Nd-YAG laser operating at a wavelength of 1064 nm and a pulse width of 7 ns (full width at half maximum), was used to deliver the laser energy. A black tape was used as the ablative coating and BK7 glass was used as the transparent confinement.

Note that in addition to high density of deformation twinning, nano-sized grains might be produced in the very top surface layer of Mg alloys by LSP [34–36]. In order to eliminate the effect of grain refinement on tribological properties, the LSP-processed samples were electrochemically polished to remove the top layer with a thickness of 50 μm. This will also eliminate the surface roughening effect induced by LSP [30]. Mg alloy samples with various TVFs were prepared by electrochemical polishing of laser-processed samples to remove the top layer with a series of thickness from 50 to 450 μm, as shown in Fig. 1b. All the samples subjected to tribological tests were polished to reach a surface roughness less than 100 nm and then ultrasonically cleaned by acetone.

2.3. Microstructure characterization and hardness tests

The twinning microstructure was characterized using Leica DM2700 optical microscopy (OM), JEOL-7100FT field emission scanning electron microscope (FESEM), and electron backscattered diffraction (EBSD). Samples for OM and FESEM characterization were prepared by sectioning, mounting, polishing, and chemical etching. The solution used for etching was a mixed acetic picral solution (10 ml acetic acid + 4.2 g picric acid + 10 ml distilled water + 70 ml ethanol). The well-polished samples were immersed into the solution for 10 s and then washed by ethanol and dried by a heater fan [37]. EBSD scans were performed with HKL Channel 5 data acquisition software on an area of 200 μm by 200 μm with a step size of 0.5 μm. All the microstructure characterization was performed on a cross-section perpendicular to the normal direction (ND). In-depth hardness was measured from the top surface to a depth of 600 μm using a Wilson Hardness tester with a 500 g load and 10s dwelling time.

2.4. Tribo-performance tests

Tribological properties of the Mg alloy samples were tested using a pin-on-plate sliding configuration using an R-Tech Muti-Functional Tribometer at room temperature in air with a relative humidity of about 20%. The experimental setup is schematically illustrated in Fig. 2. The cylindrical pin with a hemispherical tip (a diameter of 0.25 in.) was made of an aluminum alloy 6061 (AA6061) with a Vickers hardness of 110 VHN. Dry sliding tests were conducted on the surface of Mg alloy samples with different TVFs. Applied loads of 10, 20, 30, 50 N and a sliding velocity of 2 mm/s were used in the tests. The variation of COF values with sliding distance for each specimen was recorded. After sliding tests, the worn surface morphologies of both the Mg alloy substrate and AA6061 pin were characterized using three-dimensional (3-D) optical profilometer, SEM, and energy dispersive spectroscopy (EDS).

3. Results

3.1. Gradient twinning microstructure generated by LSP

Fig. 3 shows gradient twinning microstructure in an AZ31B Mg alloy generated by LSP. The originally equiaxed grains with a strong basal texture now contain a high density of deformation twins that are in a gradient distribution through the thickness can be observed in the top surface layer of the laser-processed sample (as shown in Fig. 3a). A number of needle-like twin lamellas (with a dark brown color after etching) can be identified in the OM images showing microstructure at a depth of 0, 100, and 150 μm (Fig. 3b). With the increase of depth, fewer twins can be observed. At the depth of 350 μm, most of the grains contain almost no twins. The TVF can be measured by dividing the area of twins to the overall area by ImageJ software based on color difference between twins and parents [38]. Fig. 3c shows TVF vs. depth from the top surface. It can be seen that the TVF decreases from 38% at a depth of 50 μm to 0% at a depth of 350 μm.

The formation of the gradient twinning microstructure is attributed to the gradient plastic strain in laser-processed samples [23]. In the LSP

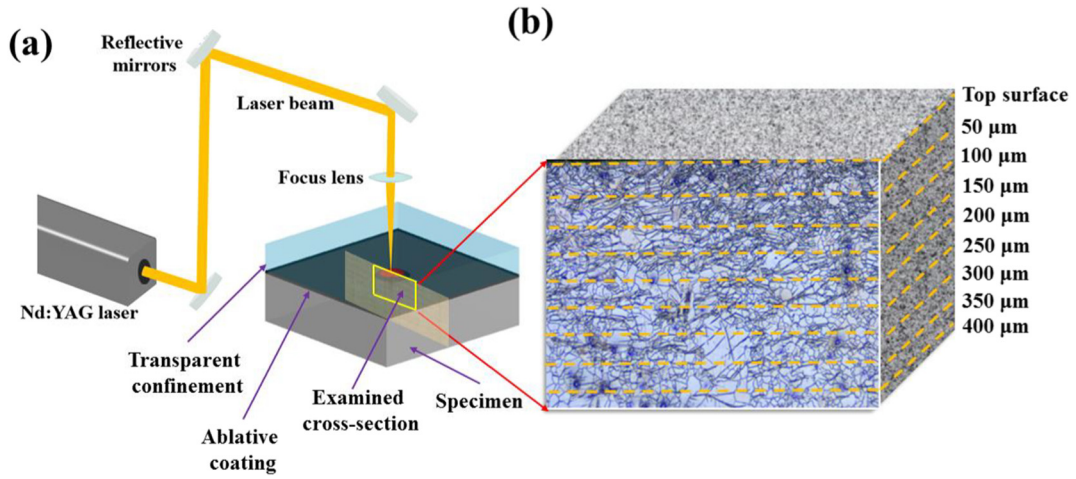

Fig. 1. Schematic illustrations of (a) the LSP process and (b) preparation of Mg alloy samples with different TVFs.

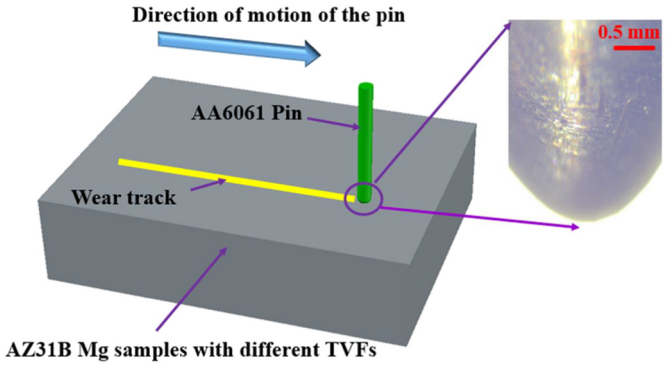

Fig. 2. Schematic illustration of the pin-on-plate test.

process, the laser-induced shockwave propagates into the material and decays with increasing depth, leading to a gradient plastic strain distribution in the surface of as-processed samples [39–41]. The relationship between the plastic strain and the magnitude of TVF can be expressed as: $\varepsilon_{twin} = f_{twin} \times \gamma_{twin} \times m$, where ε_{twin} denotes the macroscopic strain, f_{twin} is the TVF, γ_{twin} is the magnitude of twinning shear, and m is the average Schmid factor of the twinning systems [42,43]. The variation of TVF might influence the friction and wear performance of Mg alloys through affecting the surface strength, dislocation slip, and subsequent twinning processes [44–46].

EBSD analysis was performed to study the twinning microstructure of laser-processed sample at a depth of 100 μm. The inverse pole figure map in Fig. 4a shows that a large number of twin lamellas are formed in the parent grains which exhibit a basal texture. The crystallographic orientation of one twin variant and the parent grain in Fig. 4b shows the misorientation between twin and parent is about 86°, indicating that the twinning type is $\{10\bar{1}2\}\langle 10\bar{1}\bar{1}\rangle$ tension twin [47]. Different types of twin boundaries with specific misorientation angles are highlighted by different colors in the image quality map as shown in Fig. 4c. The dominant twin boundaries are 86 ± 5°$\langle 11\bar{2}0\rangle$ (in blue) representing $\{10\bar{1}2\}\langle 10\bar{1}\bar{1}\rangle$ extension twins. The red twin boundaries (only very few) are 56 ± 5°$\langle 11\bar{2}0\rangle$, representing $\{10\bar{1}1\}\langle 10\bar{1}\bar{2}\rangle$ contraction twins. The yellow boundaries are 60 ± 5°$\langle 10\bar{1}0\rangle$, which are generated when different extension twin variants interact. The green boundaries are 38 ± 5°$\langle 11\bar{2}0\rangle$, representing the $\{10\bar{1}1\} + \langle 10\bar{1}2\rangle$ double twins. Obviously, the extension twins are the dominant twinning mode. Moreover, {0002} pole figure map in Fig. 4d shows that several twin variants have been activated, which is consistent with results in the previous studies which state that several twin variants could be activated under ultra-high strain-rate deformation [48,49].

3.2. Effect of TVF on friction coefficient

Fig. 5 shows the effect of TVF on the COF as measured by the sliding tests with a load of 20 N and a sliding velocity of 2 mm/s. Fig. 5a and b show COFs with sliding distance for the samples with a TVF of 0% and 38%, respectively. It is found that the value of COF more or less remains constant with sliding distance for both samples. Moreover, with an increase of TVF from 0% to 38%, the mean value of COF is decreased by around 50% from 0.148 to 0.072. Fig. 5c shows that the friction value gradually decreases with the increase of TVF. For instance, the COF values for the samples with a TVF of 8% and 24% are 0.135 and 0.112, respectively. The experimental results in Fig. 5 indicate that the friction performance of Mg alloy is highly affected by the twinning microstructure in terms of TVF.

3.3. Effect of TVF on wear performance

The 3-D profiles of the worn surface of the AZ31B Mg alloy with different TVFs after sliding tests under an applied load of 20 N are presented in Fig. 6a–d. It can be seen the wear tracks are composed of grooves along the sliding direction. Material is displaced to the two sides of the wear tracks due to the plowing effect during dry sliding. To quantitatively compare the effect of TVF on the wear performance of AZ31B Mg alloys, cross-sectional profiles of the worn surfaces of the samples with different TVFs are summarized in Fig. 6e. It is found that the average wear track depth decreases with the increase of TVF. For instance, the wear track depths are around 1.76 and 0.55 μm for the sample with a TVF of 0% (free of twins) and 38%, respectively. This indicates the wear volume has been significantly reduced by the presence of high density extension twins. Moreover, it is found that the height of the material displaced to the sides of wear track for the sample with a TVF of 0% (0.4 μm) is much larger than that of the sample with a TVF of 38% (0.15 μm), demonstrating a stronger plowing effect during the sliding test for the sample with a lower TVF.

Wear rates of samples with different TVFs as affected by applied loading in the sliding tests are shown in Fig. 7. It can be seen that the wear rate increases with the increase of applied loading for all samples. For instance, as the load increases from 10 to 50 N, the wear rate increases from 9.24×10^{-5} to $82.15 \times 10^{-5}\, mm^3/cm{\cdot}N$ for the sample with a TVF of 0%. Since AA6061 pin has a much higher surface microhardness as compared to Mg alloys, increasing applied load causes a higher degree of plowing of softer counterpart [4]. Moreover, the wear rate decreases as the TVF increases at all loading circumstances. For example, given the applied loading of 50 N, the wear rate is reduced by 58% from 82.15×10^{-5} to $31.32 \times 10^{-5}\, mm^3/cm{\cdot}N$ as the TVF increases from 0% to 38%. Figs. 6 and 7 demonstrate the effect of TVF on

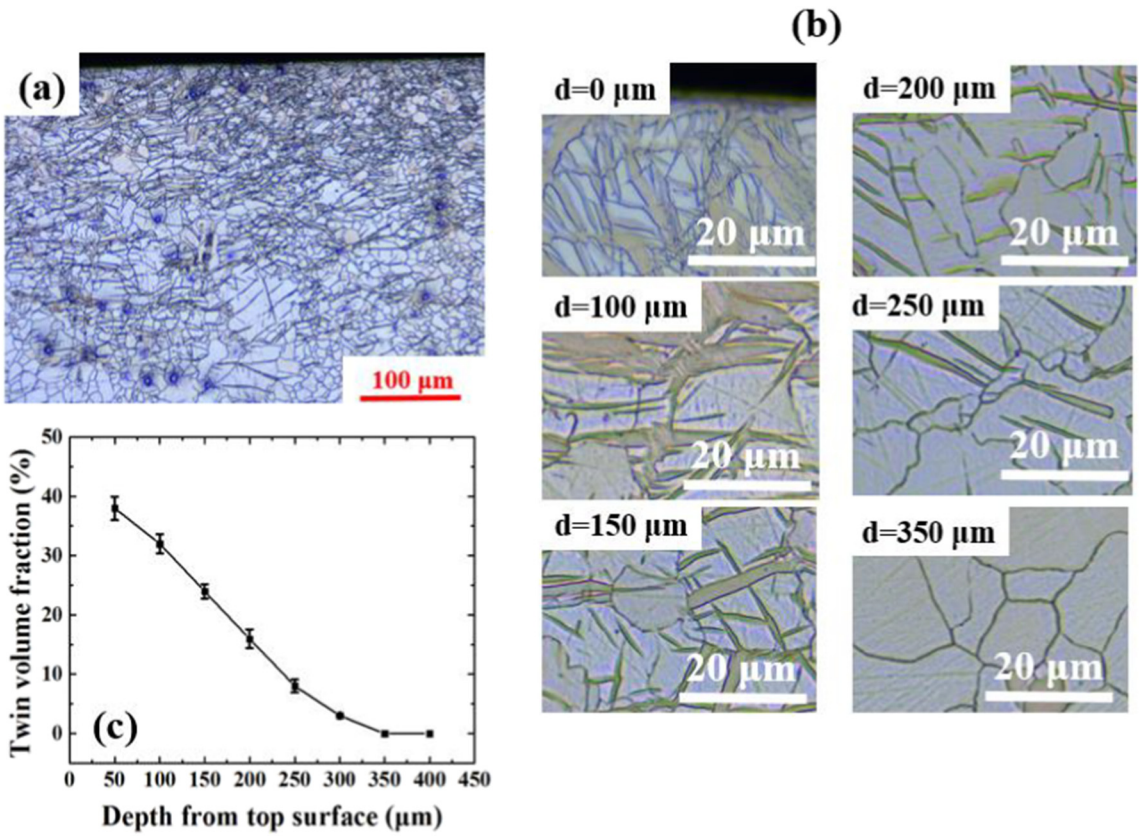

Fig. 3. Twinning microstructure in an AZ31B Mg alloy generated by LSP: (a) an OM image showing gradient twinning microstructure, (b) OM images showing various TVFs at different depths, and (c) TVF vs. depth from top surface.

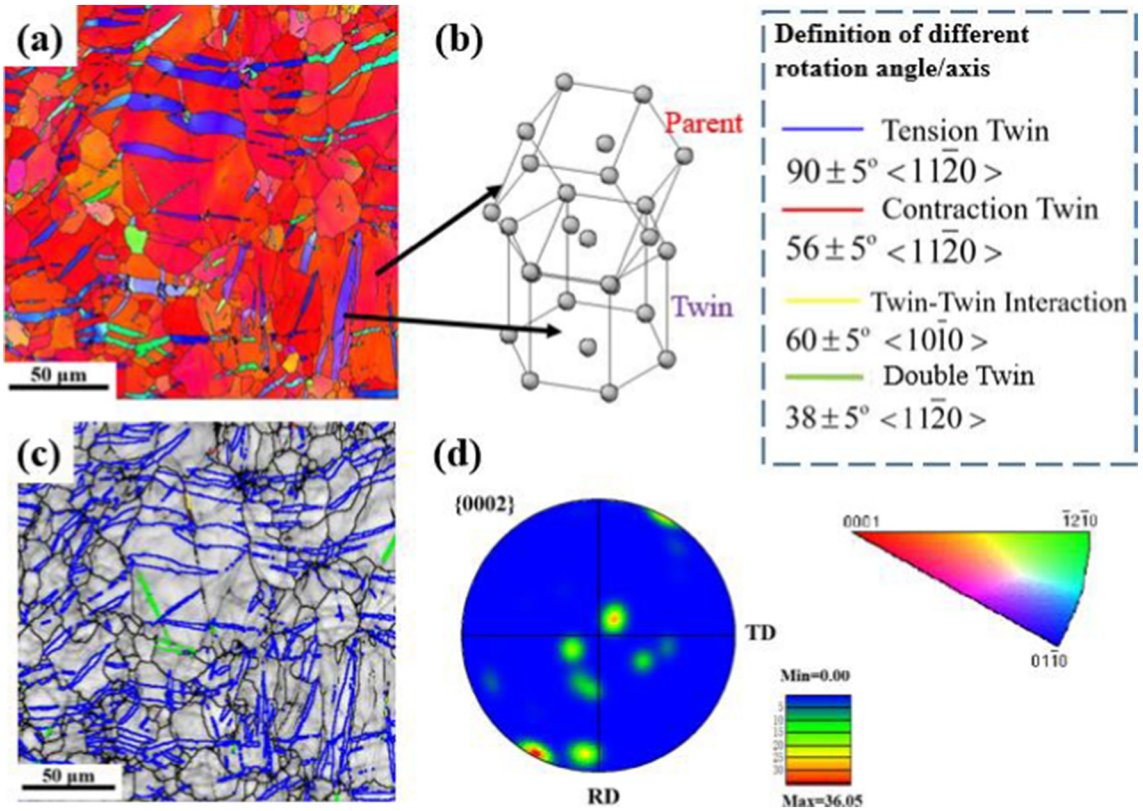

Fig. 4. EBSD analysis of the microstructure of laser-processed Mg alloy at a depth of 100 μm with a TVF of 30%. (a) Inverse pole figure map; (b) the misorientation between the parent and the twin crystals; (c) Quality map in which different types of twin boundaries are highlighted; (d) {0002} pole figure.

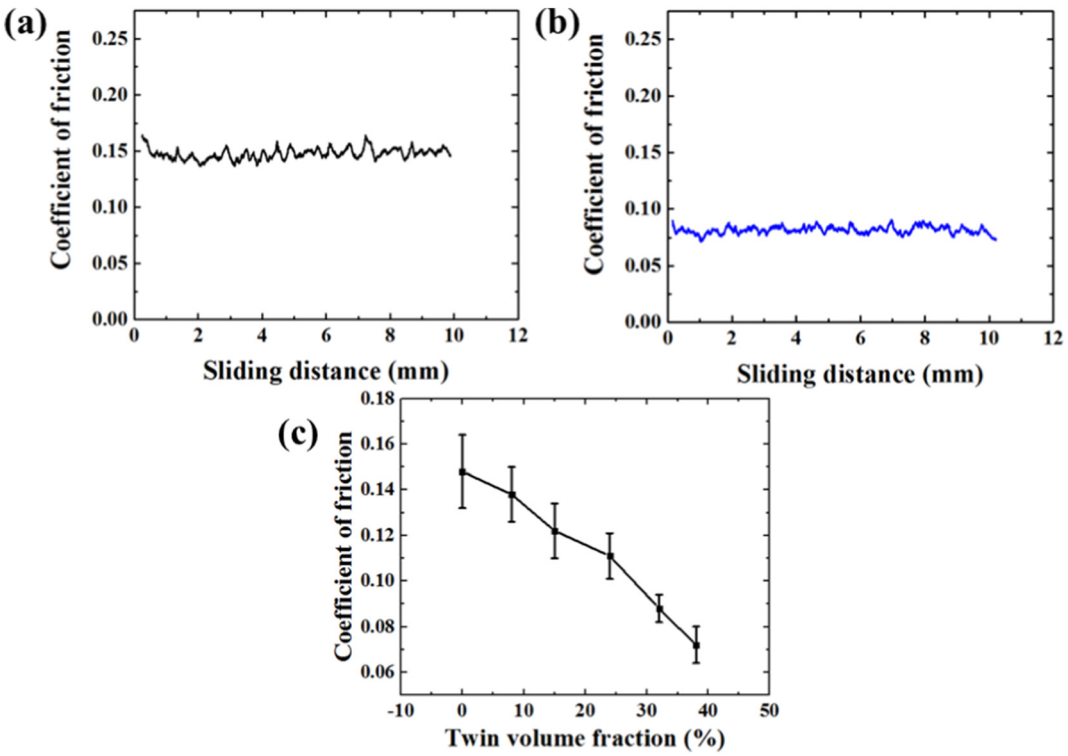

Fig. 5. Effect of TVF on the COF of Mg alloy samples in sliding tests under the load of 20 N. (a) and (b), COFs of samples with TVF of 0% and 38%, respectively; and (c) COF vs. TVF.

the enhanced wear resistance of Mg alloy.

4. Discussion

4.1. Effect of deformation twinning on friction

The COF has two components, i.e. the adhesion component and the plowing component. The adhesion component depends on the material pair, lubrication and also on the real area of contact, while the plowing component depends on the "degree of plastic deformation" taking place at the asperity level [50–52]. The twin-induced surface hardening effect is expected to change the real area of contact and the degree of plastic deformation and thus influence the COF between the AA6061 pin and Mg alloy as a function of TVF [53].

To understand the effect of deformation twinning on the COF, Vickers micro-hardness tests were conducted on the surface of Mg alloy samples with different TVFs, as shown in Fig. 8. The hardness value of the AA6061 pin is also indicated in the figure for comparison. It can be seen that the micro-hardness value of Mg sample gradually increases with the TVF. For instance, the Vickers hardness number (VHN) increases from 62 to 72 VHN as the TVF increases from 8% to 38%. The twinning-induced hardening of Mg alloys has been reported by several studies [54–56] and two mechanisms are assumed to be responsible for the improved hardness. The first mechanism is dynamic Hall-Petch effect. Twins subdivide the parent grains and induce a grain refinement effect [54]. The other is texture hardening. The presence of twins can change the surface crystallographic texture as $\{10\bar{1}2\}\langle 10\bar{1}\bar{1}\rangle$ twinning reorients the parent lattice by nearly 90° (Fig. 4). Thus, the orientation of the parent grains is changed from an easy-to-deform direction to a difficult-to-deform direction [57]. As the surface hardness of Mg alloy increases with the increase of TVF, the hardness difference between the tribo-pair of AA6061 pin and Mg alloy substrate decreases. This means that the plowing of AA6061 pin (and thus the frictional force) in the Mg sample decreases with the increase of TVF. Therefore, a higher TVF in Mg alloys lead to a lower COF.

4.2. Effect of deformation twinning on wear

To study the effect of deformation twinning on the wear behavior of Mg alloys, the worn surfaces after sliding tests were analyzed by SEM. Fig. 9 shows micrographs and EDS analysis of the worn surfaces for the samples with a TVF of 0% or 38% after sliding tests under the load of 20 N. Large numbers of grooves on the wear tracks along the scratch direction can be observed in Fig. 9a and c. The width of the wear track for the sample with a TVF of 0% is around 297 μm, which is wider than that of the sample with a TVF of 38% (253 μm in width). Moreover, the higher magnification image (Fig. 9b) of the sample with 0% TVF indicates that there are coarse wear debris and delamination damage on the worn surfaces. In contrast, the size of wear debris on the worn surface of the sample with 38% TVF is much finer as shown in Fig. 9d, and no apparent delamination can be observed. The EDS analysis shows that the chemical compositions of the wear debris in both samples are mainly magnesium and oxygen. According to the wear mechanism of Mg alloys as discussed in [10,11,13,58], the dominant wear mechanisms in the current study are abrasion together with delamination and oxidation. When the aluminum pin slides against the Mg alloy substrate, the softer counterpart (Mg alloy) is subjected to wear and oxidation due to the plowing and frictional heating [58]. More importantly, by comparing the width of wear tracks (Fig. 9a and c) and the size of wear debris (Fig. 9b and d), it can be concluded that both the abrasive wear and delamination wear in AZ31B Mg alloy have been significantly reduced by increasing the TVF.

The contact surfaces of the AA6061 pins were also examined by EDS phase mapping. Fig. 10a–c and d–f show the results for the Al, Mg, and O signals on the tip surfaces of the AA6061 pins after sliding against the Mg alloy substrates with TVF of 0% and 38%, respectively. The scratching tests were conducted with a normal load of 20 N. It can be seen that a substantial amount of Mg was transferred to the AA6061 pin surfaces in both cases, and the contact area of Mg is consistent with the width of the wear tracks in Fig. 9. Moreover, oxidation is involved during the sliding process, as shown in Fig. 10c and f. The amount of

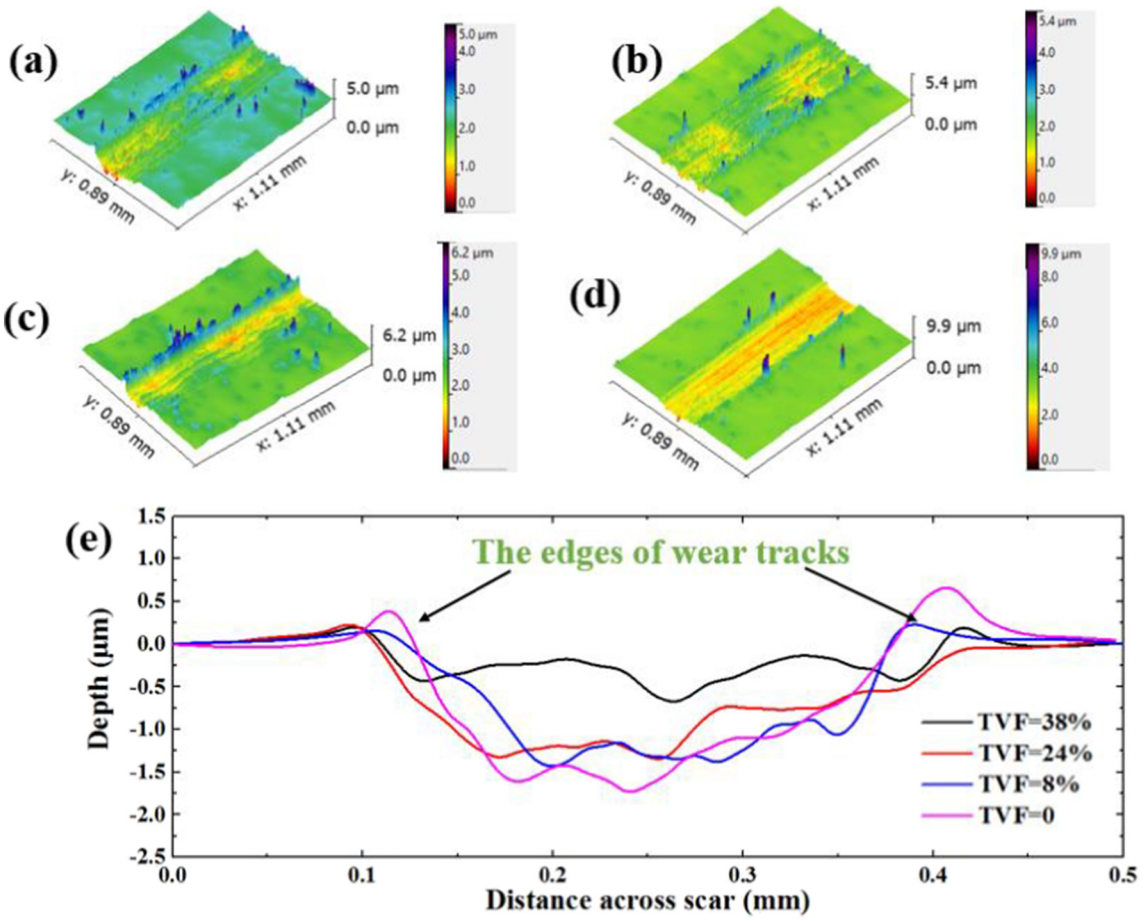

Fig. 6. Surface profiles of wear tracks of the samples with different TVFs subjected to sliding tests under an applied load of 20 N: (a) TVF = 38%, (b) TVF = 24%, (c) TVF = 8%, and (d) TVF = 0 (free of twins); and (e) cross-sectional profiles of the worn surfaces of the samples with different TVFs.

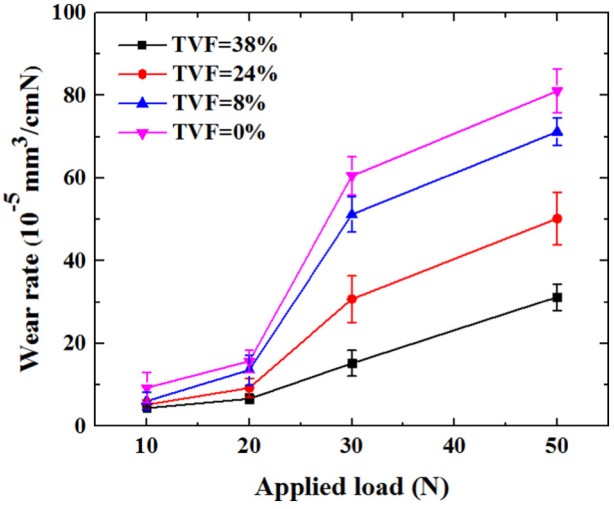

Fig. 7. Wear rates of samples with different TVFs as affected by applied loading in the sliding tests.

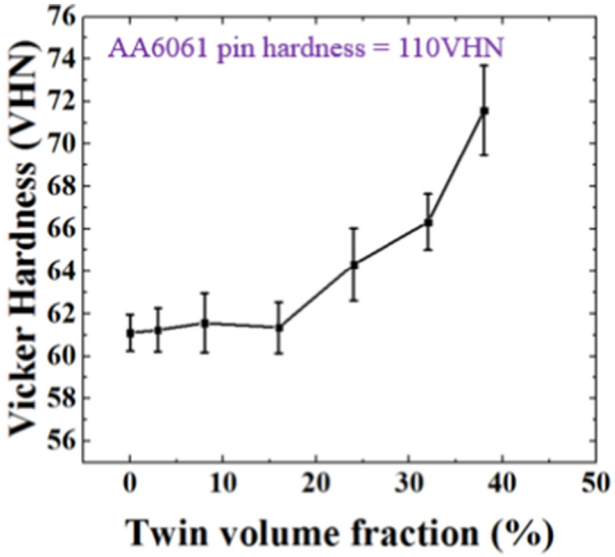

Fig. 8. Variation of surface micro-hardness values of Mg alloy samples with TVF. The hardness value of AA6061 pin is also indicated in the figure for comparison.

Mg and O elements observed in Fig. 10e and f are lower than that in Fig. 10b and c, indicating the sample with a TVF of 38% exhibits a greater wear resistance (less plowing) as compared to the sample with free of twins.

According to the Archard's law [59], the relationship between the hardness of the wear volume can be described as: $V = \frac{LkW}{H}$, where V is the wear volume, L is the sliding distance, W is the normal load, H is the hardness of the softer material in the contacting pair, and k is the wear coefficient. Given the twinning-induced hardening effect, the wear volume is expected to be reduced substantially by the presence of twins. It can be seen that although the wear depth is more than three times for

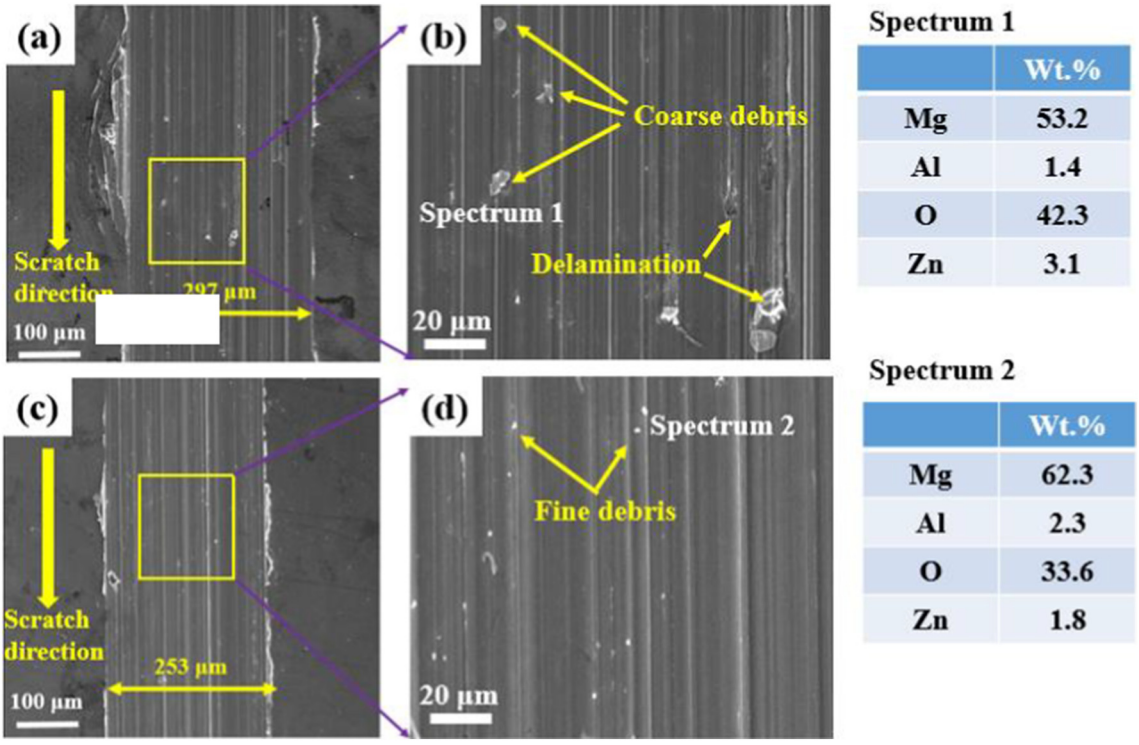

Spectrum 1

	Wt.%
Mg	53.2
Al	1.4
O	42.3
Zn	3.1

Spectrum 2

	Wt.%
Mg	62.3
Al	2.3
O	33.6
Zn	1.8

Fig. 9. SEM images and EDS analysis of worn surfaces of samples with a TVF of (a) 0% and (c) 38%; images (b) and (d) correspond to the locally enlarged figures for (a) and (c); and spectrum 1 and 2 correspond to the wear debris in (b) and (d), respectively.

the surface with free of twins as compared to the surface with a TVF of 38%, the hardness is improved only by 16.1%. This indicates that apart from the improved surface hardness by the presence of twins, other factors such as twinning-induced surface crystallographic texture change [57] might also contribute to the enhanced wear resistance.

4.3. Proposed mechanism

To reveal the mechanism of the effect of TVF on the tribological behavior of Mg alloys, the subsurface microstructure of Mg alloy samples (TVF = 0% and 38%) before and after sliding tests were characterized using SEM and EBSD. As shown in Fig. 11a, the sample free of twins exhibits the microstructure prior to deformation in which no twin can be identified. After the sliding test, a wear track is generated on the sample surface (Fig. 11c). Fig. 11b shows the microstructure of sample with TVF of 38%. After the sliding test, a wear track is also observed (Fig. 11d). EBSD analysis was carried out to study the microstructure beneath the wear tracks of the samples after sliding tests. The inverse pole figure maps for samples TVF of 0% and 38% are shown Fig. 11e and f, respectively. The corresponding {0002} pole figure maps are shown in Fig. 11g and h. For the sample without twins, it can be observed in Fig. 11e that an area with high density twins (TVF is

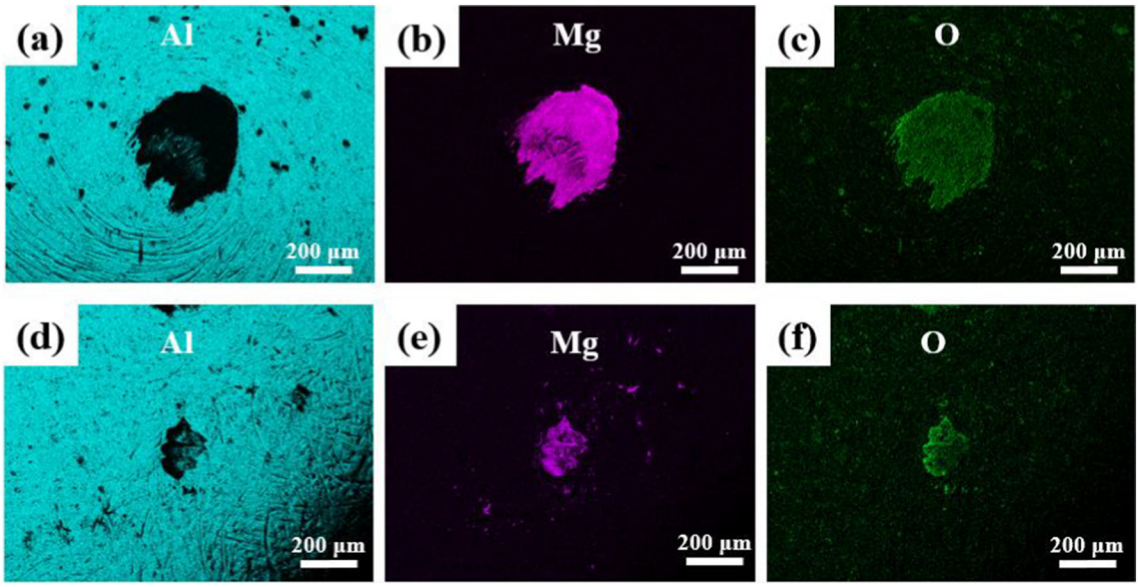

Fig. 10. EDS phase mapping results of the (a, d) Al signal, (b, e) Mg signal, and (c, f) O signal for the tip surface of the Al pins after sliding against the Mg alloy substrates with free of twins (a, b, c) and with a TVF of 38% (d, e, f).

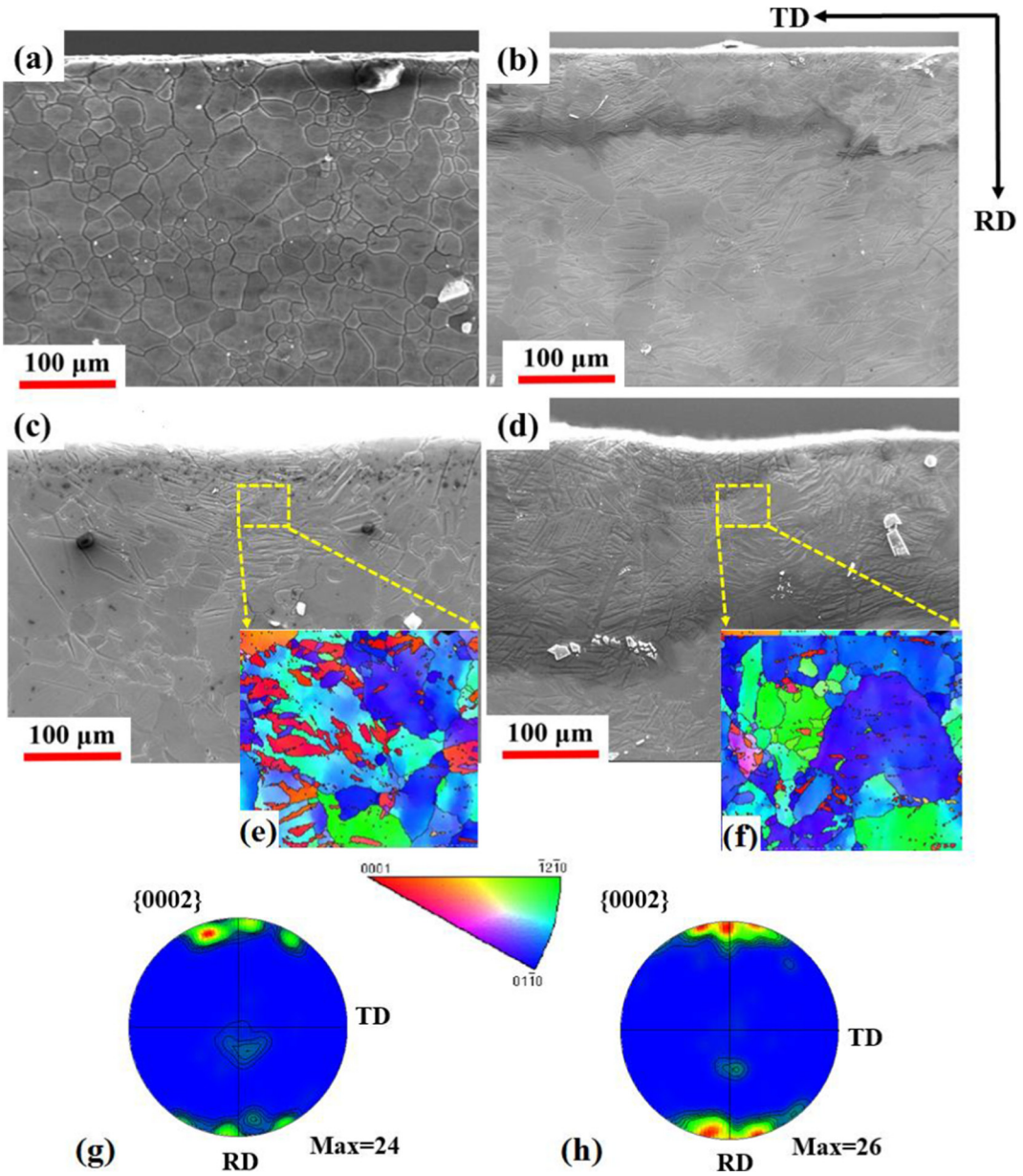

Fig. 11. SEM images of microstructure of samples with a TVF of 0% and 38% before (a and b) and after (c and d) sliding tests, respectively; EBSD analysis of the microstructure beneath the wear track: inverse pole figure maps and {0002} pole figure maps of samples with a TVF of 0% (e and g) and 38% (f and h) after sliding tests, respectively.

estimated to be around 80%) beneath the wear track is revealed after sliding tests. The nucleation and growth of the twins beneath the wear track is caused by the plastic deformation induced by the penetration of the AA 6061 pin to the Mg alloy substrate. Similar observations were reported by Liang et al. [18]. For the sample with a TVF of 38%, TVF dramatically increases to almost 100% after sliding tests (Fig. 11f), indicating that the occurrence of extensive twin-growth activities till twin saturation. Note that the samples free of twins exhibit a strong basal texture as shown in our previous study [23]. The {0002} pole figures in Fig. 11g and h imply that the crystallographic texture of the microstructure has been significantly changed with the growth and saturation of twins during sliding tests. This twin growth and saturation and twinning-induced surface crystallographic texture change during sliding motion of Mg alloys might contribute to the change of COF and wear resistance.

Based on the above analysis and discussion, the mechanism responsible for the influence of TVFs on COF and wear resistance of Mg alloy is proposed and schematically illustrated in Fig. 12. Fig. 12a–b and c–d show the contacting and sliding conditions between tribo-pair of AA6061 pin and AZ31 substrate with a low TVF and a high TVF, respectively. The red hexagons represent the grains prior to deformation (Fig. 12a) which have a strong basal texture, and the blue lamellas (Fig. 12c) represent the pre-existing twins introduced by LSP processing before sliding. The blue hexagons (Fig. 12d) and green lamellas (Fig. 12b and d) represent the fully twinned grains and newly developed twins in the sliding tests, respectively. As shown in Fig. 12b, twinning is responsible for the plastic deformation of the substrate when the AA6061 pin is penetrated into it. However, for the sample with a high TVF (Fig. 12c), subsequent twinning (growth of pre-existing twins and nucleation of new twins) occurs until the microstructure near the wear track is fully twinned (Fig. 12d). Non-basal slip systems with higher critical resolved shear stresses need to be activated to accommodate further plastic deformation during sliding (Fig. 12d) [60,61]. Therefore, the penetration depth and the contacting area of the

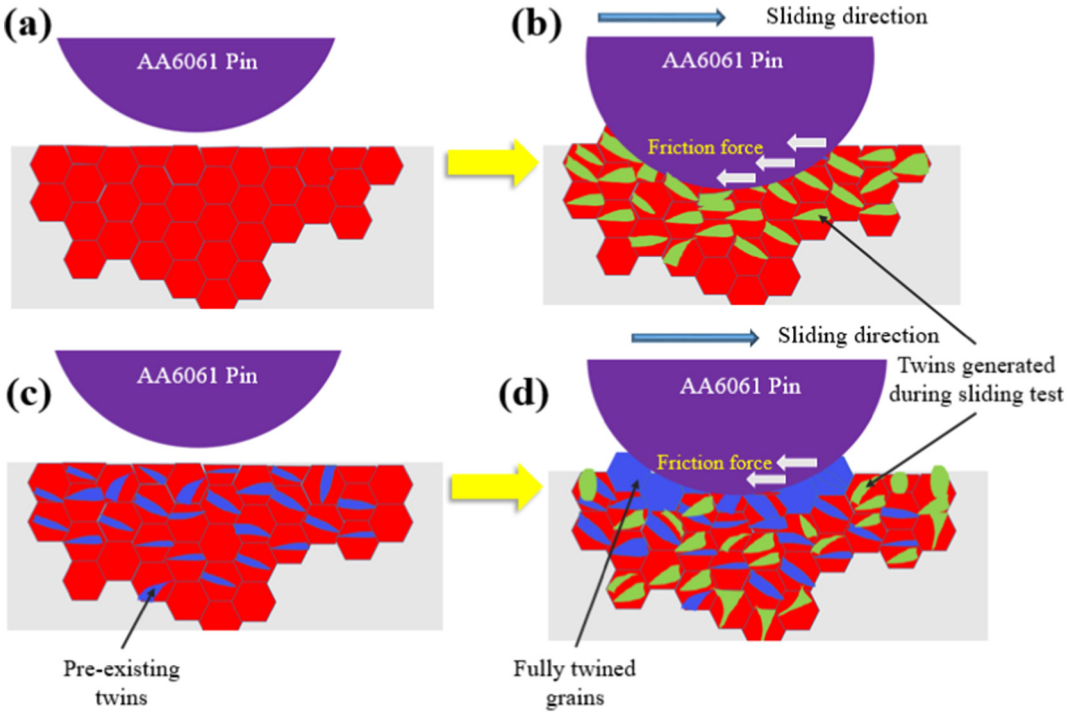

Fig. 12. Schematic illustration of proposed mechanism responsible for the influence of TVFs on COF and wear resistance of Mg alloy: AA6061 pins sliding against the surfaces of Mg alloy with (a, b) a low TVF and (c, d) a high TVF.

aluminum pin against the substrate in Fig. 12d are smaller than those in Fig. 12b. As a result, the plowing effect in Mg alloy samples with a high TVF (Fig. 12d) is weaker than that in samples with a low TVF (Fig. 12b), resulting in a lower COF and reduced wear volume [29,62,63]. Similarly, for samples with a higher TVF, saturation of twinning and activation of non-basal slip should occur earlier than that for samples with a lower TVF, leading to a more prominent effect in reducing the COF and enhancing the wear resistance.

5. Conclusions

In this work, the influence of surface pre-twinning on the tribological performance of an AZ31B Mg alloy is investigated. Sliding tests are performed on surfaces with different TVFs under dry condition. The microstructure of the worn surface and subsurface of Mg alloy samples after sliding tests are characterized and analyzed. The relationships among the TVF, COF, and wear resistance are discussed. Following conclusions can be drawn:

(1) Pre-twinning on Mg alloys can bring a surface hardening effect. A higher TVF results in a greater surface hardness number due to the twinning-induced hardening effect.
(2) The COF decreases with the increase of TVF in Mg alloy samples.
(3) The wear resistance increases with the increase of TVF in Mg alloys.
(4) Twin growth/saturation and twinning-induced crystallographic texture change are observed beneath the wear track of Mg alloy samples after sliding tests.
(5) The mechanism responsible for the influence of pre-twinning on COF and wear resistance of Mg alloy is proposed. It is discussed that the reduced COF and enhanced wear resistance of Mg alloy with increase of TVF are attributed to the twinning-induced hardening effect, twin growth and saturation phenomenon, and twinning-induced surface crystallographic texture change during the sliding.

We envision that the knowledge of twinning effect on tribological properties of Mg alloys gained in this study can offer new insights on the designing and developing Mg alloys towards enhanced tribological performance.

Acknowledgements

The authors appreciate the financial support by startup funding from the Department of Mechanical Engineering at the University of Nevada, Reno. Y. Liao appreciates the support by ORAU Ralph E. Powe Junior Faculty Enhancement Award, 2016. B. Li thanks the support from US National Science Foundation (CMMI-1635088).

The raw/processed data required to reproduce these findings cannot be shared at this time as the data also forms part of an ongoing study.

References

[1] T.M. Pollock, Weight loss with magnesium alloys, Science 328 (2010) 986–987.
[2] Y. Ogawa, D. Ando, Y. Sutou, J. Koike, A lightweight shape-memory magnesium alloy, Science 353 (2016) 368–370.
[3] H.E. Friedrich, B.L. Mordike, Magnesium Technology, Springer, 2006.
[4] H. Chen, A. Alpas, Sliding wear map for the magnesium alloy Mg-9Al-0.9 Zn (AZ91), Wear 246 (2000) 106–116.
[5] T. Mukai, M. Yamanoi, H. Watanabe, K. Higashi, Ductility enhancement in AZ31 magnesium alloy by controlling its grain structure, Scr. Mater. 45 (2001) 89–94.
[6] Q. Huo, X. Yang, H. Sun, B. Li, J. Qin, J. Wang, J. Ma, Enhancement of tensile ductility and stretch formability of AZ31 magnesium alloy sheet processed by cross-wavy bending, J. Alloys Compd. 581 (2013) 230–235.
[7] C. Cai, S. LingHui, D. XingHao, W. BaoLin, Enhanced mechanical property of AZ31B magnesium alloy processed by multi-directional forging method, Mater. Charact. 131 (2017) 72–77.
[8] H. Zhang, G. Huang, L. Wang, H.J. Roven, F. Pan, Enhanced mechanical properties of AZ31 magnesium alloy sheets processed by three-directional rolling, J. Alloys Compd. 575 (2013) 408–413.
[9] P.J. Blau, M. Walukas, Sliding friction and wear of magnesium alloy AZ91D produced by two different methods, Tribol. Int. 33 (2000) 573–579.
[10] C. Taltavull, B. Torres, A. Lopez, J. Rams, Dry sliding wear behavior of AM60B magnesium alloy, Wear 301 (2013) 615–625.
[11] J. An, R. Li, Y. Lu, C. Chen, Y. Xu, X. Chen, L. Wang, Dry sliding wear behavior of magnesium alloys, Wear 265 (2008) 97–104.
[12] S. Ramanathan, Dry sliding wear behavior of as-cast ZE41A magnesium alloy, Mater. Des. 31 (2010) 1930–1936.
[13] C. Taltavull, P. Rodrigo, B. Torres, A. López, J. Rams, Dry sliding wear behavior of AM50B magnesium alloy, Mater. Des. 56 (2014) 549–556.
[14] T. Itoi, K. Gonda, M. Hirohashi, Relationship of wear properties to basal-plane

texture of worn surface of Mg alloys, Wear 270 (2011) 606–612.
[15] H. Sun, Y.-N. Shi, M.-X. Zhang, Wear behaviour of AZ91D magnesium alloy with a nanocrystalline surface layer, Surf. Coat. Technol. 202 (2008) 2859–2864.
[16] Y. Liu, B. Jin, D.-J. Li, X.-Q. Zeng, J. Lu, Wear behavior of nanocrystalline structured magnesium alloy induced by surface mechanical attrition treatment, Surf. Coat. Technol. 261 (2015) 219–226.
[17] S. Wang, Z. Yang, Y. Zhao, M. Wei, Sliding wear characteristics of AZ91D alloy at ambient temperatures of 25–200 °C, Tribol. Lett. 38 (2010) 39–45.
[18] C. Liang, C. Li, X. Lv, J. An, Correlation between friction-induced microstructural evolution, strain hardening in subsurface and tribological properties of AZ31 magnesium alloy, Wear 312 (2014) 29–39.
[19] L. Yu, J. Cao, Y. Cheng, An improvement of the wear and corrosion resistances of AZ31 magnesium alloy by plasma electrolytic oxidation in a silicate–hexametaphosphate electrolyte with the suspension of SiC nanoparticles, Surf. Coat. Technol. 276 (2015) 266–278.
[20] Y. Yang, H. Wu, Improving the wear resistance of AZ91D magnesium alloys by laser cladding with Al–Si powders, Mater. Lett. 63 (2009) 19–21.
[21] B. Li, E. Ma, Atomic shuffling dominated mechanism for deformation twinning in magnesium, Phys. Rev. Lett. 103 (2009) 035503.
[22] J.W. Christian, S. Mahajan, Deformation twinning, Prog. Mater. Sci. 39 (1995) 1–157.
[23] B. Mao, Y. Liao, B. Li, Gradient twinning microstructure generated by laser shock peening in an AZ31B magnesium alloy, Appl. Surf. Sci. 457 (2018) 342–351.
[24] N. Guo, B. Song, C. Guo, R. Xin, Q. Liu, Improving tensile and compressive properties of magnesium alloy rods via a simple pre-torsion deformation, Mater. Des. 83 (2015) 270–275.
[25] B. Song, N. Guo, T. Liu, Q. Yang, Improvement of formability and mechanical properties of magnesium alloys via pre-twinning: a review, Mater. Des. 62 (2014) (1980-2015) 352–360.
[26] P. Peyre, R. Fabbro, Laser Shock Processing: A Review of the Physics and Applications, Optical and Quantum Electronics, vol. 27, (1995), pp. 1213–1229.
[27] C.S. Montross, T. Wei, L. Ye, G. Clark, Y.-W. Mai, Laser shock processing and its effects on microstructure and properties of metal alloys: a review, Int. J. Fatigue 24 (2002) 1021–1036.
[28] A. Claverie, J. Deroy, M. Boustie, G. Avrillaud, A. Chuvatin, E. Mazanchenko, G. Demol, B. Dramane, Experimental characterization of plasma formation and shockwave propagation induced by high power pulsed underwater electrical discharge, Rev. Sci. Instrum. 85 (2014) 063701.
[29] B. Mao, A. Siddaiah, P.L. Menezes, Y. Liao, Surface texturing by indirect laser shock surface patterning for manipulated friction coefficient, J. Mater. Process. Technol. 257 (2018) 227–233.
[30] A. Siddaiah, B. Mao, Y. Liao, P.L. Menezes, Surface characterization and tribological performance of laser shock peened steel surfaces, Surf. Coat. Technol. 351 (2018) 188–197.
[31] X. Zhang, Y. Zhang, J. Lu, F. Xuan, Z. Wang, S. Tu, Improvement of fatigue life of Ti–6Al–4V alloy by laser shock peening, Mater. Sci. Eng. A 527 (2010) 3411–3415.
[32] J. Wang, Y. Zhang, J. Chen, J. Zhou, M. Ge, Y. Lu, X. Li, Effects of laser shock peening on stress corrosion behavior of 7075 aluminum alloy laser welded joints, Mater. Sci. Eng. A 647 (2015) 7–14.
[33] R. Zhang, X. Zhou, H. Gao, S. Mankoci, Y. Liu, X. Sang, H. Qin, X. Hou, Z. Ren, G.L. Doll, The effects of laser shock peening on the mechanical properties and biomedical behavior of AZ31B magnesium alloy, Surf. Coat. Technol. 339 (2018) 48–56.
[34] M.-Z. Ge, J.-Y. Xiang, Z. Fan, Y. Lu, W. Lei, Effect of laser energy on microstructure of Mg-3Al-1Zn alloy treated by LSP, J. Alloys Compd. 734 (2018) 266–274.
[35] X. Ren, J. Huang, W. Zhou, S. Xu, F. Liu, Surface nano-crystallization of AZ91D magnesium alloy induced by laser shock processing, Mater. Des. 86 (2015) 421–426.
[36] S. Lou, Y. Li, L. Zhou, X. Nie, G. He, W. He, Surface nanocrystallization of metallic alloys with different stacking fault energy induced by laser shock processing, Mater. Des. 104 (2016) 320–326.
[37] S. Fatemi-Varzaneh, A. Zarei-Hanzaki, H. Beladi, Dynamic recrystallization in AZ31 magnesium alloy, Mater. Sci. Eng. A 456 (2007) 52–57.
[38] M. Barnett, Twinning and the ductility of magnesium alloys: part I: “tension” twins, Mater. Sci. Eng. A 464 (2007) 1–7.
[39] J. Millett, S. Stirk, N. Bourne, G. Gray, On the behaviour of the magnesium alloy, AZ61 to one-dimensional shock loading, Acta Mater. 58 (2010) 5675–5682.
[40] G. Kanel, G. Garkushin, A. Savinykh, S. Razorenov, T. de Resseguier, W. Proud, M. Tyutin, Shock response of magnesium single crystals at normal and elevated temperatures, J. Appl. Phys. 116 (2014) 143504.
[41] B. Mao, Y. Liao, Modeling of lüders elongation and work hardening behaviors of ferrite-pearlite dual phase steels under tension, Mech. Mater. 129 (2019) 222–229.
[42] S.-G. Hong, S.H. Park, C.S. Lee, Role of {10−12} twinning characteristics in the deformation behavior of a polycrystalline magnesium alloy, Acta Mater. 58 (2010) 5873–5885.
[43] A. Ghaderi, M.R. Barnett, Sensitivity of deformation twinning to grain size in titanium and magnesium, Acta Mater. 59 (2011) 7824–7839.
[44] G. Proust, C.N. Tomé, A. Jain, S.R. Agnew, Modeling the effect of twinning and detwinning during strain-path changes of magnesium alloy AZ31, Int. J. Plast. 25 (2009) 861–880.
[45] J. Jordon, J. Gibson, M. Horstemeyer, H. El Kadiri, J. Baird, A. Luo, Effect of twinning, slip, and inclusions on the fatigue anisotropy of extrusion-textured AZ61 magnesium alloy, Mater. Sci. Eng. A 528 (2011) 6860–6871.
[46] L. Wang, G. Huang, Q. Quan, P. Bassani, E. Mostaed, M. Vedani, F. Pan, The effect of twinning and detwinning on the mechanical property of AZ31 extruded magnesium alloy during strain-path changes, Mater. Des. 63 (2014) 177–184.
[47] B. Li, X. Zhang, Twinning with zero twinning shear, Scr. Mater. 125 (2016) 73–79.
[48] V. Livescu, C.M. Cady, E.K. Cerreta, B.L. Henrie, G.T. Gray, The high strain rate deformation behavior of high purity magnesium and AZ31B magnesium alloy, Essential Readings in Magnesium Technology, Springer, 2016, pp. 375–380.
[49] K. Hazeli, V. Kannan, O. Kingstedt, G. Ravichandran, K. Ramesh, Deformation twin nucleation and twin variant selection in single crystal magnesium as a function of strain rate, arXiv preprint arXiv:1801.10252, (2018).
[50] P.L. Menezes, S.V. Kailas, Influence of surface texture and roughness parameters on friction and transfer layer formation during sliding of aluminium pin on steel plate, Wear 267 (2009) 1534–1549.
[51] P.L. Menezes, S.V. Kailas, Influence of surface texture on coefficient of friction and transfer layer formation during sliding of pure magnesium pin on 080 M40 (EN8) steel plate, Wear 261 (2006) 578–591.
[52] M. Sahin, C.S. Cetinarslan, H.E. Akata, Effect of surface roughness on friction coefficients during upsetting processes for different materials, Mater. Des. 28 (2007) 633–640.
[53] Y. Zhang, K. Wang, Z. Han, G. Liu, Dry sliding wear behavior of copper with nano-scaled twins, Wear 262 (2007) 1463–1470.
[54] P. Wu, X. Guo, H. Qiao, S. Agnew, D. Lloyd, J. Embury, On the rapid hardening and exhaustion of twinning in magnesium alloy, Acta Mater. 122 (2017) 369–377.
[55] H. Fan, S. Aubry, A. Arsenlis, J.A. El-Awady, The role of twinning deformation on the hardening response of polycrystalline magnesium from discrete dislocation dynamics simulations, Acta Mater. 92 (2015) 126–139.
[56] M. Jahedi, B.A. McWilliams, P. Moy, M. Knezevic, Deformation twinning in rolled WE43-T5 rare earth magnesium alloy: influence on strain hardening and texture evolution, Acta Mater. 131 (2017) 221–232.
[57] M. Knezevic, A. Levinson, R. Harris, R.K. Mishra, R.D. Doherty, S.R. Kalidindi, Deformation twinning in AZ31: influence on strain hardening and texture evolution, Acta Mater. 58 (2010) 6230–6242.
[58] F. Mert, Dry sliding wear behaviour of as-cast AZ31B magnesium alloy, Mechanics 23 (2017) 728–734.
[59] J. Archard, Contact and rubbing of flat surfaces, J. Appl. Phys. 24 (1953) 981–988.
[60] Y. Tang, J.A. El-Awady, Formation and slip of pyramidal dislocations in hexagonal close-packed magnesium single crystals, Acta Mater. 71 (2014) 319–332.
[61] H. Yoshinaga, R. Horiuchi, Deformation mechanisms in magnesium single crystals compressed in the direction parallel to hexagonal axis, Trans. Jpn. Inst. Metals 4 (1963) 1–8.
[62] M. Mokhtar, The effect of hardness on the frictional behaviour of metals, Wear 78 (1982) 297–304.
[63] J. Challen, P. Oxley, An explanation of the different regimes of friction and wear using asperity deformation models, Wear 53 (1979) 229–243.